Proceedings of the Society for

EXPERIMENTAL MECHANICS, INC.

Proceedings of the Society for

EXPERIMENTAL MECHANICS, INC.

(Formerly the Society for Experimental Stress Analysis)

VOLUME XLIV

K.A. Galione, Publisher
M.E. Yergin, Managing Editor

7 SCHOOL STREET
BETHEL, CT 06801
Printed in U.S.A. 1987

THE SOCIETY FOR EXPERIMENTAL MECHANICS, INC.

The Society for Experimental Mechanics, Inc. (formerly the Society for Experimental Stress Analysis) was founded in 1943 as a non-profit scientific and educational organization. Its objective is to "promote and encourage the furtherance of knowledge pertaining to experimental mechanics."

The members of SEM represent a unique network of leaders in experimental mechanics in the U.S. and abroad. They are active in academia, government and industrial research and development and include scientists, engineers, manufacturers, consultants, users and vendors of plant equipment, services and systems. SEM also maintains close contact with other professional groups throughout the world with cooperative meetings and joint membership options.

SEM is large enough to have a broad base in mechanics, yet small enough to maintain good communication between members with diverse specialties. The Technical Divisions within SEM offer interdisciplinary lines of communication and include several professional interests in Composite Materials, Fracture, Modal Analysis/Dynamic Systems, Structural Testing, Residual Stress, Optical Methods, Strain Gages, Transducers and Applied Photoelasticity. Local section meetings provide opportunities for members to meet regularly and exchange information and enjoy professional as well as social contact.

SEM sponsors Spring and Fall Conferences with exhibits, co-sponsors the International Conference on Modal Analysis (IMAC) with Union College, topical conferences and educational seminars. These, along with the monthly magazine, EXPERIMENTAL TECHNIQUES, and the quarterly journals EXPERIMENTAL MECHANICS and the INTERNATIONAL JOURNAL OF ANALYTICAL AND EXPERIMENTAL MODAL ANALYSIS, serve to meet the objectives of the Society. A comprehensive collection of technical literature is available from SEM's publication department.

For membership information contact SEM, 7 School Street, Bethel, CT 06801. (203) 790-6373.

NOTE: The opinions expressed on the following pages are those of the individual authors and do not necessarily represent the ideas of the Society for Experimental Mechanics, Inc.

Proceedings
of the Society
for Experimental
Mechanics, Inc.

Contents

Experimental Buckling of GRP Cylindrical Shells

by Ghazi Abu-Farsakh

ABSTRACT—During the setup of an experiment, errors may occur. Sources of such errors may be due to several factors which sometimes accumulate and then cause erroneous results. An experimental investigation on buckling of GRP (glass-reinforced-plastic) cylindrical shells, subject to axial compression and/or external pressure loading, has been carried out. At the beginning of the experiment, the initial geometrical imperfections were measured. Because of the small size of these quantities and the great effect these imperfections had on buckling loads, any small errors in the measurement procedure may lead to unreasonable results. Attempts have been made to detect these errors, and to identify and minimize their effect on experimental results. Tables are provided to show a comparison between the final experimental results and the corresponding theoretical ones.

List of Symbols

Ax = axial-compression load
E = elasticity modulus
p = external-pressure load
L = length of cylinder
R = radius of cylinder
T = wall thickness
u, v, w = generalized displacements in α, β, and γ directions, respectively
V = variable load, either equal to Ax or p according to the case
w_α, w_β = slopes in α and β directions, respectively
α, β, γ = curvilinear-orthogonal-shell general coordinates
ν = Poisson's ratio

Subscripts

ave = average
ex = experimental
im = imperfect
pr = perfect

Introduction

The buckling analysis of cylindrical shells under different types of loads has been the subject of many investigators.[1-5,7-9,11-16] Most of the studies are theoretical and few of them are experimental.

Investigations of the effect of the L/R (length-to-radius) ratio by Holston[10] on the compression buckling load indicate no significant effects for L/R values greater than 1.5 when coupling between shearing and extensional strains was neglected. Chehill and Cheng[5] studied the case of torsional buckling. They implemented the large deflection theory and included the effect of geometrical-shape imperfections having the form of the assumed buckling mode. Other investigators Tennyson and Muggeridge[13] studied the effect of axisymmetric-shape imperfections on buckling of anisotropic cylindrical shells utilizing Koiter's theory. In 1979 Abi-Shaheen[1] investigated the effect of initial geometric imperfections, boundary conditions, and fiber orientations. Generally, in most of these studies the main concern is the large discrepancy between theoretical and experimental buckling loads. As a result of these works, it was concluded that the initial imperfections and the boundary conditions are the principal causes in reducing the critical loads.

As a consequence of the rapid growth in the advanced technology of fiber-reinforced materials and their importance in industry and modern technology, more attention is being paid to the study of the behavior of structures made of such materials. Thus, the main objective of the present paper is to detect sources of experimental errors and to investigate their effect on the accuracy of the measured initial geometric imperfections. The secondary objective is to improve experimental buckling results by minimizing the potential effect of these errors.

The experimental buckling loads are compared with the corresponding theoretical loads resulting from the finite-element computer program NONL5 which utilizes the nonlinear shell theory.[2] The results show an acceptable comparison on which the present approaches are justified.

Test Specimens

The test specimens are cylindrical shells made of glass-reinforced-plastic (GRP)-type woven roving cloth (WR: - warp:weft = 1:1) embedded in heat-resistant polyester resin. Twenty test specimens were studied. These were divided into four groups each of the same nominal dimensions. The nominal length-to-radius ratio (L/R) ranges from one to four, as shown in Table 1.

The shell wall is of a composite construction consisting of three layers of equal nominal thickness (0.30 mm each) with the same fiber orientations (0 deg/0 deg/0 deg).

Experiment Modeling

The test rig (Figs. 1 and 2) was modeled in such a way that the GRP cylinders can be tested under axial compression and/or external pressure loads. In order to achieve the desired loading, the following features were considered in the design of the test rig. (1) The compression load was to be transmitted axially and as uniformly

Ghazi Abu-Farsakh (SEM Member) is Assistant Professor, Department of Civil Engineering, Yarmouk University, Irbid, Jordan.

Original manuscript received: April 22, 1985. Final manuscript received: April 15, 1986.

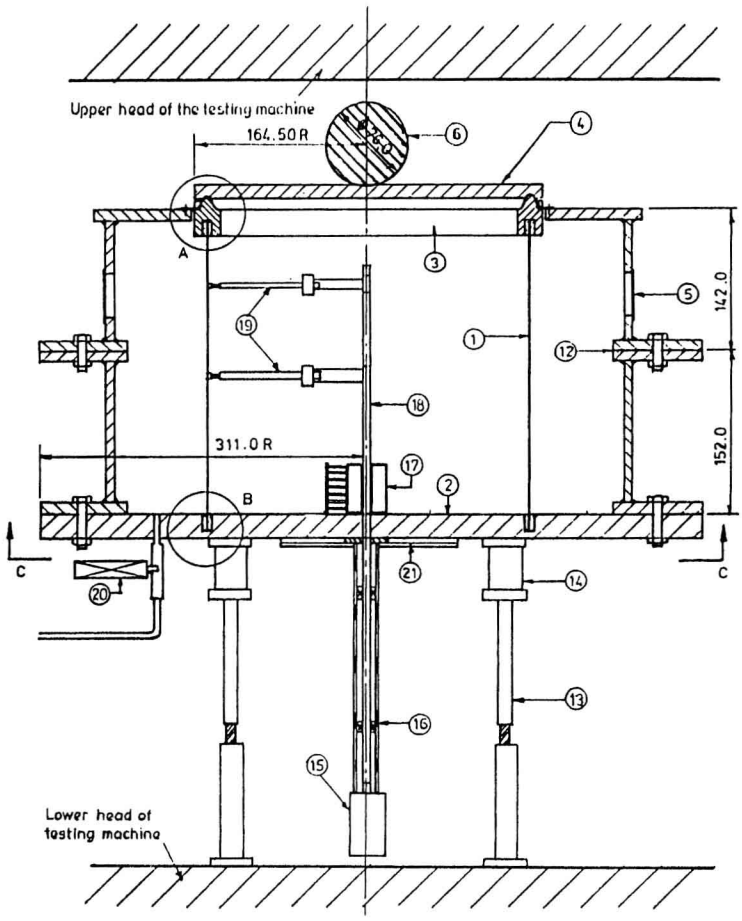

Fig. 1—Detailed drawing of the pressure-testing rig (section D-D). Plan C-C shows the position of the load cells LC1, LC2, LC3 and the heaters H1, H2 in the steel-base plate. Detail A shows the top end fixity. Detail B shows the bottom end fixity

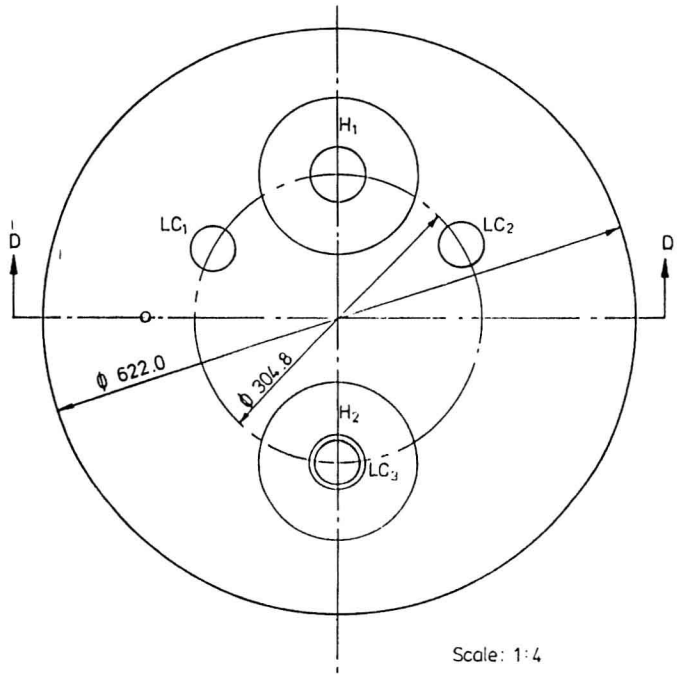

Plan C-C Showing the position of the load cells LC_1, LC_2, LC_3 and the heaters H_1, H_2 in the steel base plate.

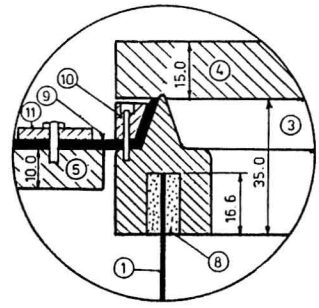

Detail - A
Showing top end fixity

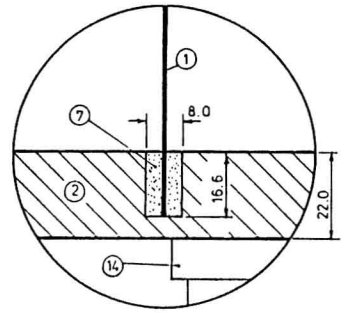

Detail B
Showing bottom end fixity. Scale 1:1

as possible to the test cylinder. (2) The space around the test cylinder was enclosed and adequately sealed so that the required pressure could be reached. (3) The height of the test rig could be varied in steps of 6 in. (152.65 mm) to allow testing of the four groups. (4) The edges of each test cylinder were built-in in order to provide the fixed-end boundary conditions.

Loading Procedure

The cylinders were tested under three types of loads.

Axial-Compression Load

The axial-compression load (Ax) was applied by a 5000-kN Mohr and Federhaff testing machine. Because of the high capacity of this machine, the axial-compression load was controlled manually by using a special technique to rotate the motor which drives the upper head of the testing machine.

The load was applied in approximately five increments with an increment size of 2, 4, or 8 kN depending upon the total expected load. In order to assist in uniformly distributing the pressure, due to the axial load the head of the ring (3) was inserted in the circular groove of the steel plate (4). The stainless-steel ball (6) of 76.0-mm diameter rested in a concave depression in the center of the plate (4). This arrangement ensured as far as possible the symmetry and uniformity of the applied axial load. Furthermore, the three screw jacks (13) under the base plate provided an extra tool to ensure a higher degree of symmetry and uniformity of the axial load.

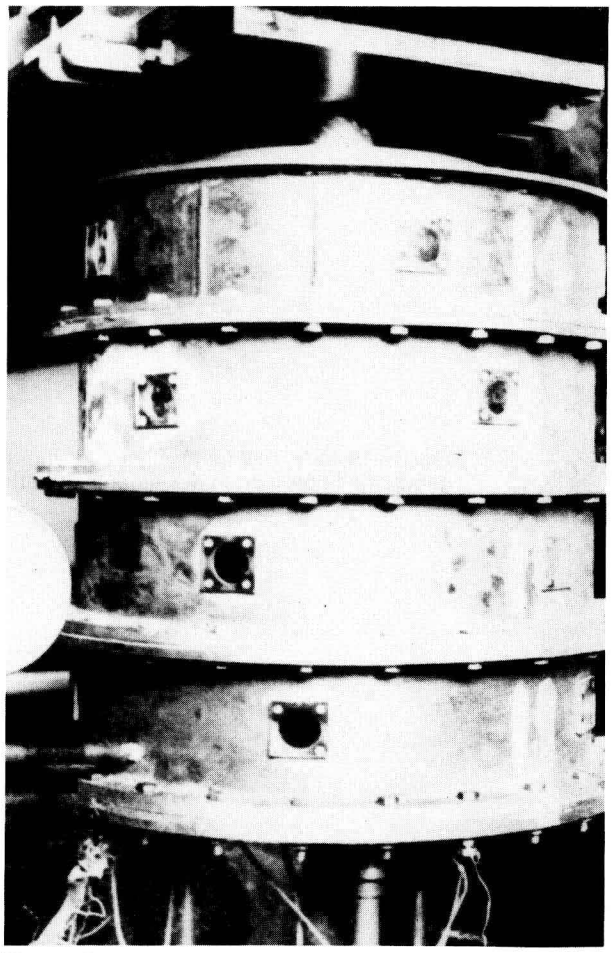

Fig. 2—Pressure testing rig (as used in the case of cylinder Group IV)

External-Hydrostatic Air-Pressure Load

External hydrostatic loading was achieved by using the diaphragm pump Model D1 (0.40 N/mm/610 mm Hg) for general vacuum and pressure duties from the same unit using a simple screw-on attachment. The pump was connected to the control valve (John Watson, Type MR3/1/SR/240 with synchronous motor) using a plastic tube. The valve was linked to an interface system (Inlab) which in turn was connected to an Intertec Data Systems Corporation microcomputer. The valve gave a regulated air pressure (p) within 0.0035-0.115 N/mm.

Combined Axial-Compression and External-Hydrostatic Air-Pressure Load

Combined axial-compression and external-hydrostatic loading was achieved by combining both above-mentioned cases of loading, either using a constant axial compression (Ax) combined with a variable external pressure (p) or vice versa.

Mounting Procedure and Instrumentation

A special testing rig was designed, as shown in Fig. 1, for the purpose of providing an enclosed space around the cylindrical specimens. The sides of the rig were sealed properly using asbestos gaskets (12). The cylindrical shell (1) was mounted on the circular steel base plate (2) with the bottom edge lying in the circular groove (7) (see detail B) which had been machined in it. The top edge of the cylinder was lying in another circular groove (8) in the steel ring (3). Both the top and the bottom grooves were filled with the low-melting-point alloy (MCP-70)*—which has the property of melting at 70°C—to provide end fixity. Two circular electric heating plates (21) were fixed under the base plate with their centers aligned symmetrically on the same diameter (see plan C-C of Fig. 1).

For the purpose of providing the external air pressure on the test cylinder, four steel cylinders with flanges at both ends (5) were made so as to enclose the space around it. In the case of the cylinders of group I, one of the steel cylinders was required. All four were required in the case of the group IV cylinders. For closing the gap between the top ring (3) and the outside cylindrical casing (5), the rubber ring (9) of 2.5-mm thickness was used. The rubber ring was tightened in its position using two steel rings [the inner (10) and the outer (11)]. This technique provided a good seal and ensured that no axial load was transmitted from the ring (3) to the surrounding steel casing (5).

Measuring Procedure

The main unit was a multipurpose control board (Inlab interface system, 3D-Digital) consisting of (a) eight channels for strain and load-cell measurements, (b) eight channels for displacement and pressure transducers, (c) two channels for stepper-motor controllers, and (d) one channel for a

*Mining and Chemical Products Ltd., U.K.

pressure-valve controller of a synchronous motor drive. Accordingly, the measurement devices can be divided into two types.

Displacement-Measurement Devices

Two linear-displacement transducers (19) (RDP transducers, Type LVDT, D5/200 AG, Grade A1) were used to measure radial geometric imperfections and radial deformations. They were held on the central stainless-steel tube (18) of high-precision dimensions by using clamping screws. The tube was aligned vertically by two self-aligning ball bearings (16).

The stepper-motor (15) (1.8 deg/step) was placed centrally at the bottom of the tube. The signal from the displacement transducer was transmitted through the slip ring and brush unit (17) and received by the interface system. The stepper-motor was used in double steps (3.6 deg) to rotate the central shaft with two transducers on it around the circumference of the cylinder.

The cylinder length, at any one position, was divided into six equal parts so that the actual shape of the cylinder circumference can be traced. With respect to measuring the initial geometric imperfections, the two transducers were placed opposite to each other (one from the inside and the other from the outside, as shown in Fig. 3) at the specified station. Stations were numbered in an increasing sequence from top to bottom (from 0 to 6). See Fig. 5(a). Rotating the transducers one complete revolution in steps of 3.6 degrees, a complete revolution equals 100 steps. During the deformation, displacements were measured, simultaneously, at stations 1 and 3 from the inside (i.e., one transducer at station 1 and the other at station 3).

Load-Measurement Devices

To measure the axial compression load, three load cells (14) placed at the top of the three screw-jacks (13) were used. At each loading increment the screw jacks were adjusted so that the load cells gave equal readings.

To measure the external hydrostatic air pressure, one pressure transducer (20) (RDP-Electronics, Type P5/50) was fixed on the inlet of the testing rig under the base. The pressure transducer was connected to the control valve which in turn was connected to the interface system. Another mechanical pressure gage was connected to the lower steel cylinder of the testing rig which served the purpose of rechecking the pressure inside.

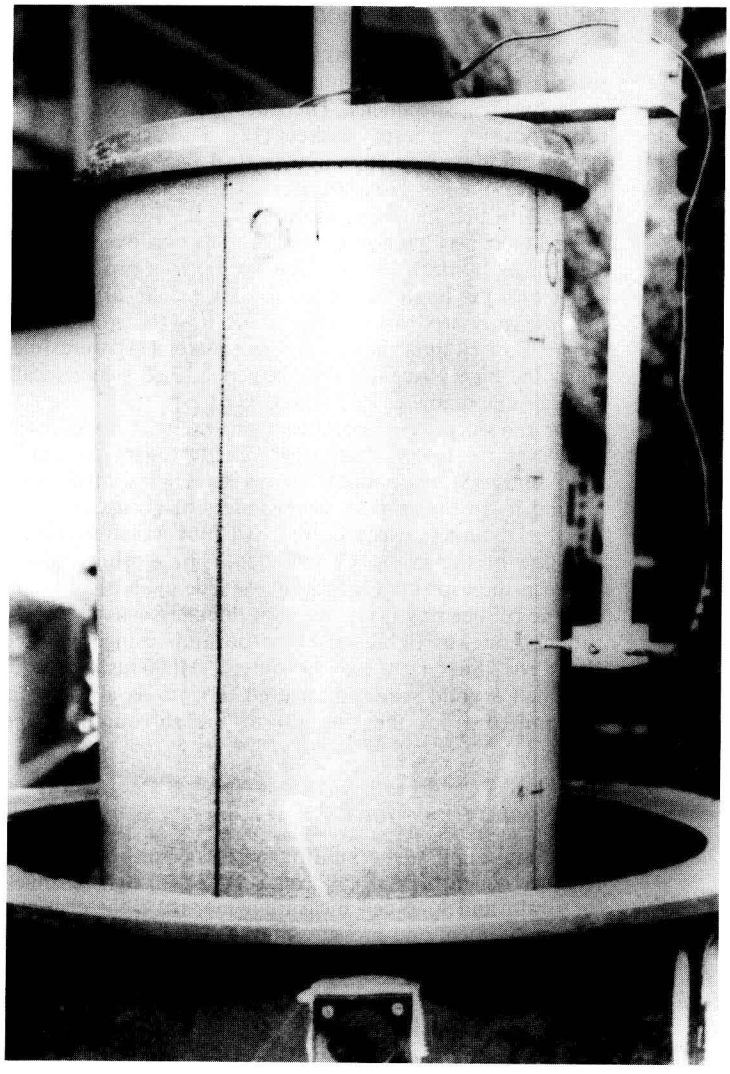

Fig. 3—Cylinder I/IV before test showing the geometric-imperfection measurement method

Analysis of Experimental Results

All the experimental results were stored on disks on the microcomputer. The circumference of each cylinder was traced and plotted at different stations before and after deformation. A computer program, RESULT, which was written in Basic, was used to analyze the geometric data. This program also provides drawings of longitudinal cross sections to show the shape of the actual cylinder wall at specific steps. As an example, the results for cylinder 4/IV (cylinder number 4 in group IV) are illustrated in Fig. 5.

Setting-Up Problems

Many problems may arise during the set-up of an experiment. In the present experiment, such problems centered around (a) measurement of initial imperfections and (b) providing a proper end fixity.

Initial Imperfections

Initial imperfections are small accidental deviations from the assumed perfect initial shape of the structure. These small deviations may be due to geometrical irregularities in the shape of the structure, variations of wall thickness, and very small misalignments of the desired directions of the applied loads. The initial geometric imperfections were measured by using two displacement transducers (RDP-Electronics, Type D5/200 AG, Grade A1). Because of the small size of these imperfections, it may be difficult to measure them very accurately. In order to avoid such difficulties, the set-up procedure must satisfy certain requirements and consider certain factors.

(a) The displacement transducers (19), (Fig. 1) should be placed radially normal to the shell wall (1). (b) The stainless-steel tube (18) should be in a vertical position perpendicular to the steel-base plate (2) and pass through its center. The results of the measured imperfections for a complete circumference at one station may show large variations if one of these requirements is not satisfied. In some cases, these variations may be unreasonably greater than the normal deviations given in Table 2. Figure 4(a) shows that the largest difference between the maximum and minimum values is approximately 3 mm (i.e., the deviation is ± 1.5 mm from the average value). By comparing this value with the normal deviation given in Table 2 for this group (± 1.25 mm), we find that the deviation is greater than the normal value but within an acceptable range. (The normal deviations are based on averaging the deviations of all cylinders of the same group.) But if the deviation was unreasonable (say ± 2 mm for our case), then it would be necessary to reset-up the experiment. It was found that these variations were smaller in smaller cylinders due to the fact that the alignment error decreases. This explains also why the experimental results at lower stations showed less deviation than upper stations. [Compare Figs. 4(a), 4(b) and 4(c) for different stations.] For normal cases, the average deviations of the measured results for the four groups are shown in Table 2.

(c) The cylindrical test specimens are made of a plastic material of small thickness which made them difficult to handle during the experiment. The effect of this can be detected easily after plotting the curves representing the circumference at stations 1, 1. (The numbers indicate the positions of the two displacement transducers.) A maximum point and a minimum point with a gradual transition between them appears on each curve. This indicates that the cylinder's actual shape is oval. See Fig. 4(a). This shape can happen also due to uneven cooling of the melted alloy (which is explained below) or misalignment of the stainless-steel tube.

(d) The cylinder length may be irregular (in most cases within ± 0.50 mm) due to cutting, which for longer cylinders can cause larger errors when placed in a vertical position. This variation in cylinder length causes the cylinder to appear to be in a slightly inclined position, as shown in Fig. 5. The irregularities in length of a cylinder made of GRP is unavoidable due to the existence of fibers. Cutting the ends of a cylinder causes a small amount of damage because of separation of fibers from the resin.

These four factors, (a)-(d), combine in such a way that their effect on test results is difficult to be distinguished or separated. In an attempt to minimize their effect on the measured initial geometric imperfections, several computer plottings of the cylinder circumference (similar to those shown in Fig. 4) at different stations were initially carried out. At this stage, if test results were unreasonable (i.e., the deviations were unreasonably larger than the normal deviations stated in Table 2), a reset-up of the experiment was necessary.

(e) The cylinder wall is thin (about 1 mm), and may have tiny holes in the resin due to manufacturing imperfections. This may cause difficulty in testing the cylinders under external pressure loading because of air penetration through these holes. Consequently, the required pressure cannot be reached (especially in the case of shorter cylinders which require high pressure). This problem was solved by placing a very thin sheet of nylon (so as not to affect the cylinder's strength) on the outside wall of the cylinder to provide a sufficient seal.

Proper End Fixity

A low melting-point alloy (MCP-70) was used to provide a proper end fixity. The top end of the cylinder (1) was seated in the circular groove (8) which was machined in the steel-base plate (2). Both grooves were filled with the low melting-point alloy. This alloy has the property of melting at 70°C. After cooling down it provides a proper

TABLE 1—THE NOMINAL DIMENSIONS OF THE CYLINDRICAL SPECIMENS

Group Number	No. of Specimens	Nominal Outside Diameter, D (mm)	Nominal Thickness, t (mm)	Nominal Length L (mm)
I	5	305.8	1.00	152.65
II	5	305.8	1.00	305.30
III	5	305.8	1.00	457.95
IV	5	305.8	1.00	610.60

TABLE 2—THE NORMAL AVERAGE DEVIATIONS AT STATIONS 1, 1

Group	Deviation
I	± 0.25 mm
II	± 0.75 mm
III	± 1.25 mm
IV	± 1.75 mm

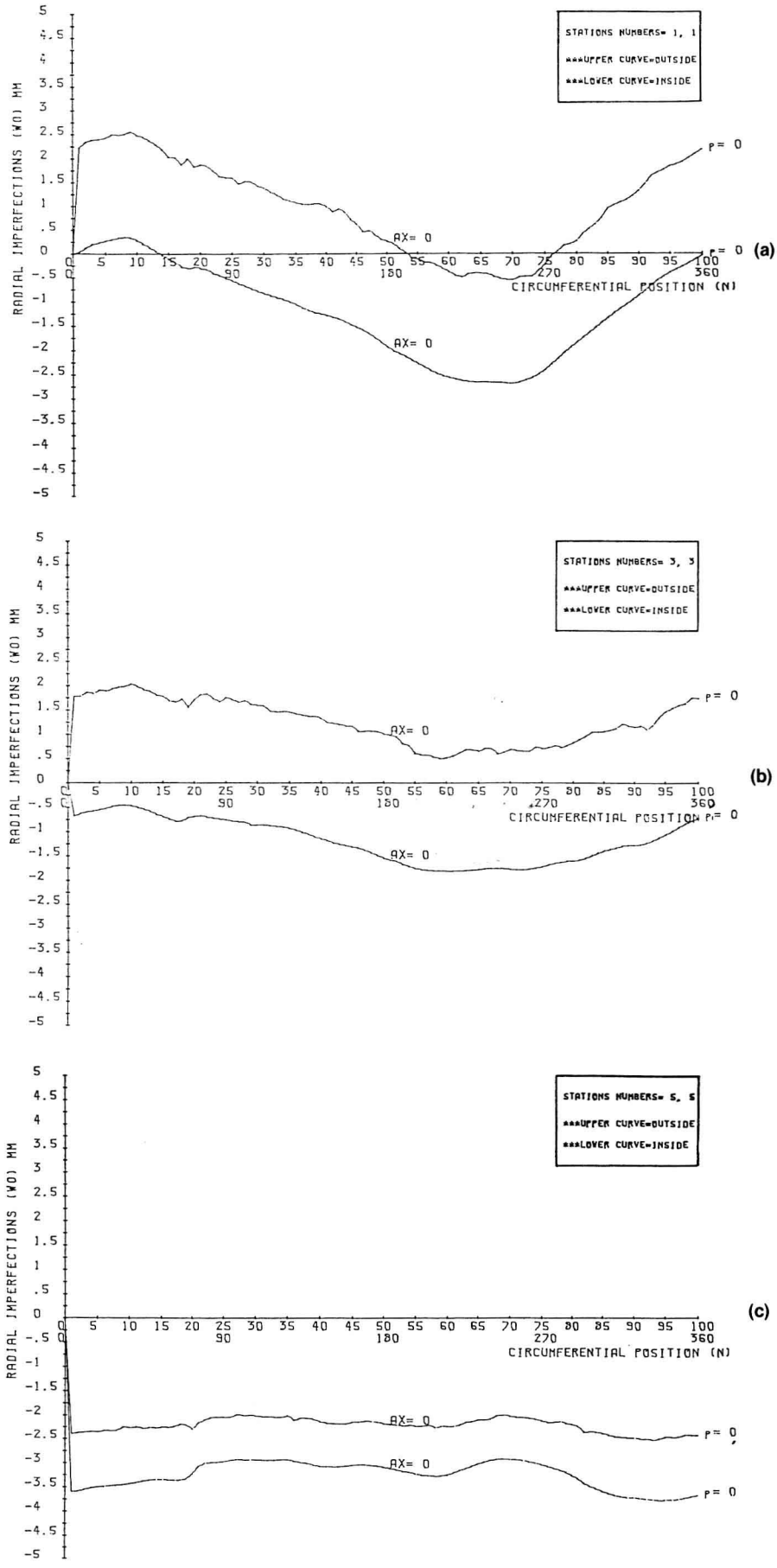

Fig. 4—Geometric imperfections (Wo) for cylinder I/III (a) at stations 1, 1; (b) at stations 3, 3; and (c) at stations 5, 5

end fixity. Using this technique, several problems may arise.

(1) Any small inclination in the base plate (2) or the upper steel ring (3) causes the melted alloy to gather at one end more than the other. To solve this problem, the base plate must be horizontal before melting the alloy. This can be achieved by using a level. The base plate can be adjusted horizontally by the aid of the three screw jacks (13) at the bottom. Further adjustment of the base can be done after melting the alloy in order to assist in distributing the material uniformly. (It is sufficient to judge uniformity of the material by the naked eye.)

(2) In order to melt the alloy, two special electric-disk heaters (21) were placed symmetrically under the base plate (as shown in plan C-C of Fig. 1). With this arrangement, the alloy in the groove can melt simultaneously and cause a uniform effect (to some extent) at the end of the cylinder when it cools down. The effect of uneven cooling (which happens if one heater is switched off before the other) may cause an ovality of the cylinder shape. Thus the deviations may increase accordingly. If this happens, it may be necessary to repeat the melting process again.

A better arrangement is to have a single heater in the center of the plate so as to assure uniform melting of the alloy. In this case, one must make sure that the stepper motor (15) can resist higher temperatures.

The effect of temperature on the strength of our GRP cylinders was not detected. But it was expected to be negligible because the polyester resin was of the heat-resistant type. (Polyester resin can resist temperatures up to 100 °C with almost no change in strength.)[17]

Comparison Between Theoretical and Experimental Results

The theoretical analysis was carried out using a non-linear analysis program (NONL5) developed by the author which utilizes the finite-element method for large-deflection elastic analysis of thin plates and shells. The element used was a ten-node triangular element with 27 degrees of freedom which implement a curvilinear orthogonal system of coordinates parallel to the sides of the triangle. The shell geometry was represented by a complete cubic polynomial which requires ten nodes for such a representation. The element displacement functions were conforming and represented by complete cubic polynomials.[2]

The accelerated modified Newton-Raphson method[6] was adopted in the analysis. It combines the advantage of a banded stiffness matrix (associated with the modified Newton-Raphson method) and the advantage of faster convergence (associated with the variable metric method). The NONL5 computer program is based on the Sanders

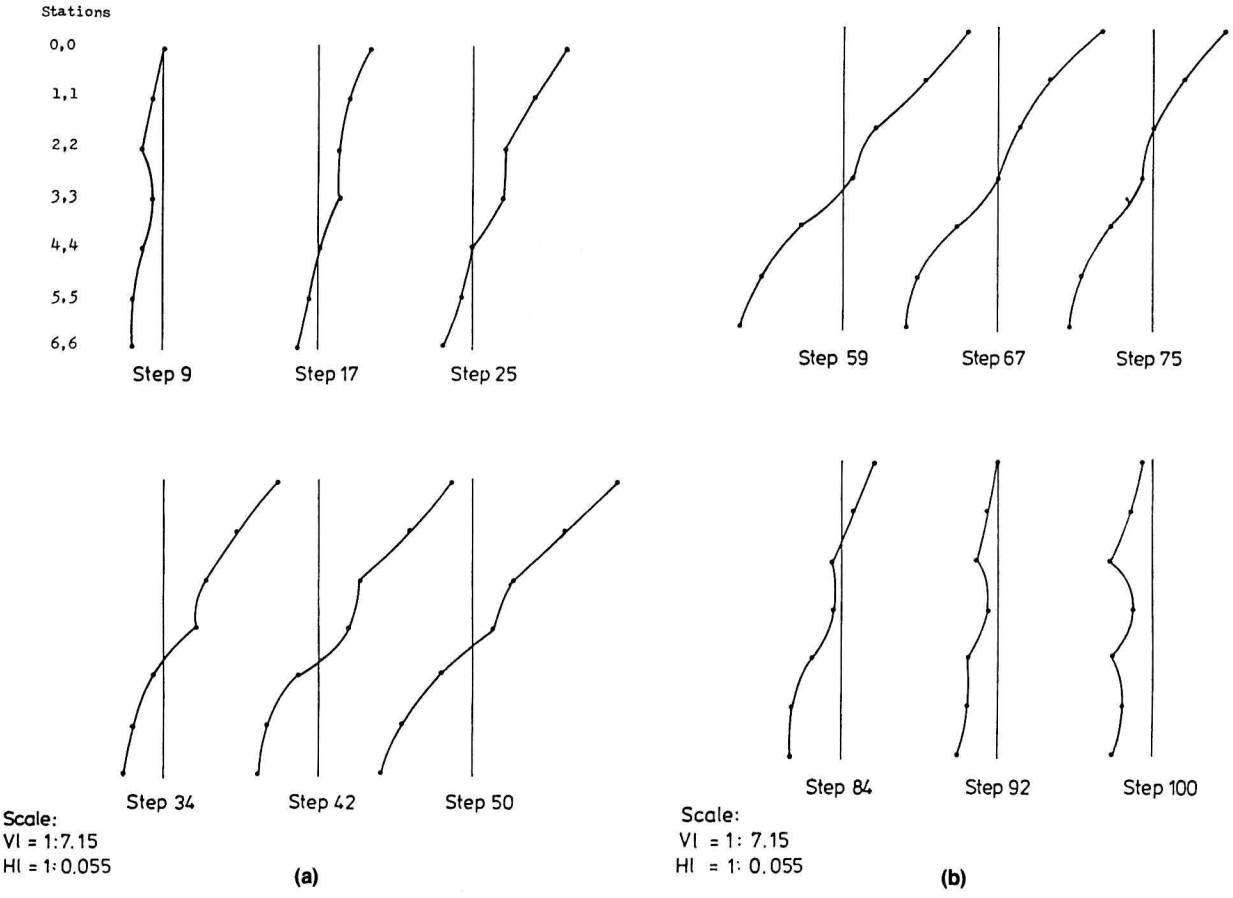

Fig. 5—Drawing of the cross sections for cylinder 4/IV

nonlinear strain-displacement relations for thin shells[10] which are valid for large displacements and moderately large rotations. The effect of geometric imperfections was introduced in such a way that the imperfection distribution was assumed to have a quadratic variation across the element. The size of the new load increment was generated depending upon the previous one according to the equation given in Ref. 2.

In analyzing the cylinders from groups III and IV, only half of the cylinder was considered using a 6 × 6 mesh (forming 72 triangular elements). In analyzing the cylinders from groups I and II the same mesh size was used to analyze a quarter of it.

In order to simulate the experimental load-deflection behavior of the combined loading case, in the theoretical analysis the constant load (either axial compression, Ax, or external pressure, p) was applied first until the total load was equal to the corresponding experimental value. Then, increments of the variable load V were applied until the buckling load was reached. ($V = p$ if the variable load is pressure. Otherwise $V = Ax$.) The boundary conditions at both ends of the cylinder were considered to be as follows.

$$v = w = w_{,\alpha} = w_{,\beta} = 0 \text{ (at both ends)}$$

$$u = 0 \quad \text{(at bottom end only)}$$

Comparisons between experimental and theoretical buckling loads are shown in Table 4. The actual dimensions of the cylinders are shown in Table 3. The results of Table 4 show an acceptable agreement between experimental and theoretical results. Reference 2 contains additional details and shows a comparison between theoretical and experimental load-deflection paths for the different cylinders.

TABLE 3a—CYLINDER GEOMETRIC AND MATERIAL PROPERTIES. (GROUPS I AND II)

Cylinder No.	R (mm)	L_{total} (mm)	L_{net} (mm)	t_{ave} (mm)	E_{ave} (N/mm²)	ν_{ave}
1/I	153.46	151.42	121.5	0.927		
2/I	153.01	153.29	117.8	0.968		
3/I	153.02	152.88	117.95	0.928	16866	0.168
4/I	153.51	153.13	119.40	0.987		
5/I	153.94	152.00	118.25	0.869		
1/II	153.47	304.51	273.01	0.881		
2/II	153.24	305.35	272.90	0.947		
3/II	153.22	305.23	272.23	0.947	15483	0.172
4/II	153.07	304.22	272.88	0.862		
5/II	153.52	305.08	273.25	0.890		

TABLE 3b—CYLINDER GEOMETRIC AND MATERIIAL PROPERTIES. (GROUPS III AND IV)

Cylinder No.	R (mm)	L_{total} (mm)	L_{net} (mm)	t_{ave} (mm)	E_{ave} (N/mm²)	ν_{ave}
1/III	153.31	458.25	424.00	0.935		
2/III	152.77	456.88	427.63	0.946		
3/III	153.20	457.00	424.00	0.974	16651	0.175
4/III	153.54	457.25	425.00	0.978		
5/III	153.42	457.38	423.75	0.952		
1/IV	153.45	610.63	576.38	0.935		
2/IV	153.58	608.88	576.63	1.000		
3/IV	153.09	609.00	576.50	0.967	17081	0.166
4/IV	153.65	609.50	577.56	0.987		
5/IV	154.03	609.63	576.00	0.987		

Conclusions

Acceptable agreement between experimental and theoretical results of buckling of glass-reinforced-plastic (GRP) cylindrical shells proves the validity and importance of the experimental technique described here.

The important effect that the initial geometric imperfections of the structure being tested has on the buckling loads of GRP cylindrical shells under axial compression is emphasized. Results show that the buckling loads under external pressure are also slightly affected by the presence of initial imperfections.

Because of their small size, many problems may occur when measuring these initial geometric imperfections. Such problems may mislead the analyst and cause erroneous results. Solving such problems mainly depends on the ability of the analyst to detect their sources and minimize their potential effect on test results.

From the theoretical analysis it is felt that the boundary conditions have greater effect on buckling of cylindrical shells under external pressure than under axial compression.

References

1. *Abi-Shaheen, S.A., "Buckling of Composite Shells of Revolution," PhD Thesis, Univ. of London, Queen Mary College (Feb. 1979).*
2. *Abu-Farsakh, G.A.R., "Analytical and Experimental Study of Buckling of Composite Shells," PhD Thesis, Univ. of London, Queen Mary College (Feb. 1983).*
3. *Adam, H.P. and King, P.A., "Experimental Investigation of the Stability of Monocoque Domes Subjected to External Pressure,"* EXPERIMENTAL MECHANICS, **5** *(10), 313-320 (Oct. 1965).*
4. *Ari-Gur, J., Baruch, M. and Singer, J., "Buckling of Cylindrical Shells Under Combined Axial Pre-Load Non-uniform Heating and Torque,"* EXPERIMENTAL MECHANICS, **19** *(11), 406-410 (Nov. 1979).*
5. *Chehill, D.S. and Cheng, S., "Elastic Buckling of Composite Cylindrical Shells Under Torsion," J. Spacecraft and Rockets,* **5** *(8), 973-978 (Aug. 1968).*
6. *Crisfield, M.A., "Iterative Solution Procedures for Linear and Non-linear Structural Analysis," Dept. of the Environment, TRRL, Crowthorne, Rep. TRRL-LR-900 (1979).*
7. *Davis, R.C. and Williams, J.G., "Buckling Experiments on Stiffened Cast-epoxy Conical Shells,"* EXPERIMENTAL MECHANICS, **15** *(9), 329-338 (Sept. 1975).*
8. *Donnell, L.H., "A New Theory for the Buckling of Thin Cylinders Under Axial Compression and Bending," Trans. Amer. Soc. Mech. Engs.,* **56**, *795-806 (1934).*
9. *Holston, A.J., "Buckling of Filament-Wound Cylinders by Axial Compression," AIAA J.,* **6** *(5), 935-936 (1968).*
10. *Sanders, J.L., "Nonlinear Theories for Thin Shells," Q. Appl. Math.,* **21** *(1), 21-36 (1963).*
11. *Singer, J., Arbocz, J. and Babcock, C.D., "Buckling of Imperfect Stiffened Cylindrical Shells Under Axial Compression," AIAA J.,* **9** *(1), 68-75 (Jan. 1971).*
12. *Sobel, L.H. and Newman, S.Z., "Plastic Buckling of Cylindrical Shells Under Axial Compression," J. Press. Vess. Tech., Trans. ASME,* **102**, *40-44 (Feb. 1980).*
13. *Tennyson, R.C. and Muggeridge, D.B., "Buckling Analysis of Laminated Anisotropic Imperfect Circular Cylinder Under Axial Compression," J. Spacecraft and Rockets,* **10** *(2), 143-148 (Feb. 1973).*
14. *Tillman, S.C., "Some Effects of Rib-reinforcement Arrangement on Spherical-dome Buckling,"* EXPERIMENTAL MECHANICS, **18** *(10), 396-400 (Oct. 1978).*
15. *Wong, L.T., Rodriquez, A.L. and Litle, W.A., "Effect of Boundary Conditions on Shell Buckling," J. Eng. Mech. Div., Proc. Amer. Soc. Civil Engs.,* **92**, *101-116 (Dec. 1966).*
16. *Yang, T.H. and Guralnick, S.A., "An Experimental Study of the Buckling of Open Cylindrical Shells,"* EXPERIMENTAL MECHANICS, **15** *(4), 121-127 (April 1974).*
17. *"Design Data-Fiberglass Composites," Fiberglass Limited, St. Helens, Merseyside, England.*

TABLE 4a—COMPARISON BETWEEN EXPERIMENTAL AND THEORETICAL BUCKLING LOADS FOR CYLINDERS OF GROUP I

Cylinder No.	Variable Load (V)*	Experimental		F.E. (NONLS)		F.E. (NONLS)		$\frac{V_{ex}}{V_{im}}$	$\frac{V_{ex}}{V_{pr}}$
		Ax_{ex} (kN)	p_{ex} (N/mm²)	Ax_{im} (kN)	p_{im} (N/mm²)	Ax_{pr} (kN)	p_{pr} (N/mm²)		
1/I	p	00.000	0.08816	00.000	0.08764	00.000	0.08807	1.006	1.001
2/I	Ax	43.126	0.00000	43.486'	0.00000	64.784	0.00000	0.992	0.676
3/I	Ax	41.187	0.00000	42.507	0.00000	60.800	0.00000	0.969	0.666
4/I	Ax	10.000	0.08779	—	—	—	—	—	—
5/I	p	00.000	0.08167	00.000	0.08589	00.000	0.08922	0.951	0.915

Notes:

*If the variable load $V = p$ then $V_{ex} = p_{ex}$, $V_{im} = p_{im}$, $V_{pr} = p_{pr}$
On the other hand, if $V = Ax$ then $V_{ex} = Ax_{ex}$, $V_{im} = Ax_{im}$, $V_{pr} = Ax_{pr}$.
'Analyzing half a cylinder.
—Indicates result is not available.

TABLE 4b—COMPARISON BETWEEN EXPERIMENTAL AND THEORETICAL BUCKLING LOADS FOR CYLINDERS OF GROUP II

Cylinder No.	Variable Load (V)	Experimental		F.E. (NONLS)		F.E. (NONLS)		$\frac{V_{ex}}{V_{im}}$	$\frac{V_{ex}}{V_{pr}}$
		Ax_{ex} (kN)	p_{ex} (N/mm²)	Ax_{im} (kN)	p_{im} (N/mm²)	Ax_{pr} (kN)	p_{pr} (N/mm²)		
1/II	Ax	37.638	0.00000	39.658	0.00000	57.373	0.00000	0.949	0.656
2/II	p	00.000	0.04417	0.000	0.03641	0.000	0.03504	1.213	1.248
							0.04112+	—	1.074
3/II	p	18.413	0.02767	—	—	18.413	0.02789	—	0.992
4/II	Ax	35.304	0.01365	37.748'	0.01365	53.630'	0.01365	0.935	0.658
5/II	p	33.489	0.01547	—	—	33.489	0.01627	—	0.951

Notes:
'Analyzing half a cylinder.
+Axial displacement u is fixed at top end.

TABLE 4c—COMPARISON BETWEEN EXPERIMENTAL AND THEORETICAL* BUCKLING LOADS FOR CYLINDERS OF GROUP III

Cylinder No.	Variable Load (V)	Experimental		F.E. (NONLS)		F.E. (NONLS)		$\frac{V_{ex}}{V_{im}}$	$\frac{V_{ex}}{V_{pr}}$
		Ax_{ex} (kN)	p_{ex} (N/mm²)	Ax_{im} (kN)	p_{im} (N/mm²)	Ax_{pr} (kN)	p_{pr} (N/mm²)		
1/III	Ax	41.884	0.00000	45.140†	0.00000	52.317†	0.00000	0.928	0.801
2/III	p	00.000	0.03135	0.000	0.02994	00.000	0.03292	1.047	0.952
3/III	p	10.560	0.02431	10.560	0.02861	10.560	0.03121	0.850	0.779
4/III	p	24.644	0.02781	24.644	0.02958	24.644	0.02680	0.940	1.037
5/III	p	29.615	0.02149	29.615	0.02116	29.615	0.02332	1.016	0.992

Notes:

*Theoretical results are obtained assuming varying axial load intensity 0.97 - 1; see Ref. 2 for more details.
†Load intensity 1.1-0.96.

TABLE 4d—COMPARISON BETWEEN EXPERIMENTAL AND THEORETICAL BUCKLING LOADS FOR CYLINDERS OF GROUP IV

Cylinder No.	Variable Load (V)	Experimental		F.E. (NONLS)		F.E. (NONLS)		$\frac{V_{ex}}{V_{im}}$	$\frac{V_{ex}}{V_{pr}}$
		Ax_{ex} (kN)	p_{ex} (N/mm²)	Ax_{im} (kN)	p_{im} (N/mm²)	Ax_{pr} (kN)	p_{pr} (N/mm²)		
1/IV	Ax	47.612	0.00000	45.080	0.00000	48.437	0.00000	1.056	0.983
2/IV	p	00.000	0.02958	00.000	0.02585	00.000	0.02754	1.144	1.074
					0.03226+		0.03314+	0.917	0.893
3/IV	p	13.861	0.23360	13.861	0.02054	13.861	0.02124	1.137	1.100
4/IV	Ax	35.520	0.01838	30.650	0.01838	32.227	0.01838	1.159	1.102
5/IV	p	21.086	0.02412	21.086	0.02346	21.086	0.02160	1.028	1.117

Notes:

+Axial displacement u is fixed at top end.